



## Abstract

This paper reports initial results from an Ozone Mapping Profiler Suite (OMPS) nadir mapper cloud pressure and cloud fraction algorithm. The OMPS cloud products are intended for use in OMPS ozone or other trace-gas algorithms. We developed the OMPS cloud products using a heritage algorithm developed for the Ozone Monitoring Instrument (OMI) on NASA's Aura satellite. The cloud pressure algorithm utilizes the filling-in of ultra-violet solar Fraunhofer lines by rotational Raman scattering. The OMPS cloud products are evaluated by comparison with OMI cloud products that have been compared in turn with other collocated satellite data including cloud optical thickness profiles derived from a combination of measurements from the CloudSat radar and the MODIS imaging radiometer. We find that the probability density functions (PDFs) of effective cloud fraction retrieved from OMPS and OMI measurements are very similar. The PDFs of the OMPS and OMI cloud pressures are comparable. However, OMPS retrieves somewhat higher pressures on average. The current NASA total ozone retrieval algorithm makes use of a monthly gridded cloud pressure climatology developed from OMI. This climatology captures much of the variability associated with the relevant cloud pressures. However, the use of actual cloud pressures retrieved with OMPS in place of the OMI climatology appears to improve OMPS total column ozone estimates slightly.

## 1 Introduction

The Ozone Mapping Profiler Suite (OMPS), flying on the Suomi National Polar-orbiting Partnership (NPP) satellite, launched by the US National Aeronautics and Space Administration (NASA) on 28 October 2011, consists of two nadir sensors and a limb profiler. The OMPS nadir sensors, the Nadir Mapper (NM) and the Nadir Profiler (NP), are designed to provide operational retrievals of total column ozone and ozone profiles. In the initial ground processing design phase, cloud pressure was not envisaged

AMTD

7, 2689–2714, 2014

## OMPS Raman cloud algorithm

A. Vasilkov et al.

Title Page

Abstract

Introduction

Conclusions

References

Tables

Figures

◀

▶

◀

▶

Back

Close

Full Screen / Esc

Printer-friendly Version

Interactive Discussion



to be an operational OMPS product; it was planned that cloud information from the Visible Infrared Imaging Radiometer Suite (VIIRS) would be utilized within the ozone algorithms.

Following the conception of the initial OMPS ozone algorithms, much has been learned about how clouds behave with respect to solar backscatter measurements such as those from OMPS. The launch of the Ozone Monitoring Instrument (OMI) on NASA's Aura satellite within the A-train afternoon constellation has provided a unique opportunity to compare cloud pressures derived with solar backscatter measurements with other nearly coincident cloud measurements including cloud optical thickness profiles retrieved with the CloudSat radar and MODerate-resolution Imaging Spectroradiometer (MODIS) radiances. For example, it is now clear that cloud pressures derived from solar backscatter measurements (henceforth referred to as cloud optical centroid pressures or OCPs) are appropriate for use in trace-gas retrievals from similar instruments (e.g., Vasilkov et al., 2004; Joiner et al., 2009); cloud top pressures (CTPs) derived from thermal measurements are not equivalent to OCPs and do not provide good estimates of solar photon pathlengths through clouds that are needed for trace-gas retrievals from ultraviolet and visible wavelength solar backscatter measurements (Joiner et al., 2006; Vasilkov et al., 2008; Ferlay et al., 2010; Joiner et al., 2012). The cloud OCP can be thought of and modelled as a reflectance-averaged pressure level reached by back-scattered photons (Joiner et al., 2012). As clouds are vertically inhomogeneous, the OCP will not necessarily be in the geometrical center of the cloud, but rather in the so-called optical centroid of the cloud (Vasilkov et al., 2008; Ziemke et al., 2009; Joiner et al., 2012); this is why we refer to the pressure as OCP. Cloud pressure information from solar backscatter measurements can be used to detect multi-layer clouds either alone (Rozanov et al., 2004) or in combination with thermal infrared measurements (Joiner et al., 2010).

The current NASA OMPS total ozone algorithm (McPeters et al., 2013) makes use of a monthly gridded climatology of cloud OCP derived from OMI rotational Raman scattering (RRS) retrievals. In this work, we apply the OMI RRS algorithm to OMPS

## OMPS Raman cloud algorithm

A. Vasilkov et al.

[Title Page](#)[Abstract](#)[Introduction](#)[Conclusions](#)[References](#)[Tables](#)[Figures](#)[◀](#)[▶](#)[◀](#)[▶](#)[Back](#)[Close](#)[Full Screen / Esc](#)[Printer-friendly Version](#)[Interactive Discussion](#)

## OMPS Raman cloud algorithm

A. Vasilkov et al.

Title Page

Abstract

Introduction

Conclusions

References

Tables

Figures

◀

▶

◀

▶

Back

Close

Full Screen / Esc

Printer-friendly Version

Interactive Discussion



radiances. Although the OMPS and OMI instruments are similar in some respects, there are substantial differences in the detailed specifications of these instruments including spectral and spatial resolutions. It was not clear at the onset whether OMPS would achieve the same level of the performance as OMI with respect to the RRS cloud retrieval. We evaluate the OMPS cloud retrievals by comparison with OMI. Since the instruments are in similar but not identical orbits, we compare the retrieved cloud parameters using probability distribution functions. We then examine whether simultaneously derived cloud OCPs from OMPS improve total column ozone retrievals as compared with the use of the OMI cloud climatology.

The paper is structured as follows: following a brief description of the OMPS NM instrument in Sects. 2 and 3 reports details of the development of the OMPS RRS cloud algorithm. Section 4.1 describes the evaluation of the OMPS cloud products. Effects of the use of actual OMPS-derived cloud OCPs on total column ozone retrievals are shown in Sect. 4.2. Conclusions are given in Sect. 5.

## 2 The OMPS Nadir Mapper (NM)

The OMPS NM employs a 2-D charge-couple device (CCD) detector that samples spectrally in one dimension and spatially in the other. It has spectral coverage from 300 to 380 nm. The spectral bandpass has a full-width at half maximum (FWHM) of  $\sim 1.0$  nm and the sampling is 0.42 nm (Flynn et al., 2006). The optical projection onto the CCD creates a “spectral smile” across the CCD where, for a given spatial row, the wavelength changes by approximately 0.2 nm from one edge of the CCD to the center, then approximate 0.2 nm back to the other edge. The spectral bandpass also varies across the swath. For comparison, OMI has spectral coverage from 270–500 nm with a FWHM of  $\sim 0.5$  nm and a spectral smile of approximately 2.0 nm from the edge to the center of the CCD and back to the other edge (Levelt et al., 2006).

The OMPS NM has a 2800 km swath width. It has a nadir footprint of 50 km  $\times$  50 km in its nominal configuration; this provides 36 pixels in the across track dimension. The

## OMPS Raman cloud algorithm

A. Vasilkov et al.

Title Page

Abstract

Introduction

Conclusions

References

Tables

Figures

◀

▶

◀

▶

Back

Close

Full Screen / Esc

Printer-friendly Version

Interactive Discussion



satellite motion provides spatial sampling in the along track dimension. The spatial sampling in the across and along tracks directions can be adjusted. During the instrument commissioning phase, the instrument has been operated at its highest possible spatial resolution ( $\sim 2.5\text{ km across track} \times 10\text{ km along track}$ ); now once per week, the instrument is operated in a high spatial resolution mode ( $10\text{ km} \times 10\text{ km}$ ). In this work, we focus on data from the nominal operating mode. The OMI swath width for comparison is  $2600\text{ km}$ , and it provides 60 pixels in the cross-track direction with a nadir footprint size of  $\sim 12\text{ km} \times 24\text{ km}$ .

### 3 OMPS RRS cloud algorithm

#### 3.1 Basic approach

Our OMPS cloud algorithm is essentially a slightly modified version of an algorithm that was developed for OMI as described in Joiner et al. (2004); Joiner and Vasilkov (2006) and Vasilkov et al. (2008). The algorithm uses the Mixed Lambert-Equivalent Reflectivity (MLER) concept that treats both cloud and ground as horizontally homogeneous opaque Lambertian-reflecting surfaces (Ahmad et al., 2004; Stammes et al., 2008). The measured top-of-the-atmosphere (TOA) radiance (normalized by the solar flux),  $I_m$ , is calculated as a sum of the clear sky and overcast (cloudy) subpixel radiances,  $I_g$  and  $I_c$ , respectively, weighted by an effective cloud fraction  $f$ , i.e.,

$$I_m = I_g(R_g) \cdot (1 - f) + I_c(R_c) \cdot f, \quad (1)$$

where  $R_g$  and  $R_c$  and the ground and cloud Lambertian-equivalent reflectivities, respectively.  $R_c$  is assumed to be 80 %; the same assumption is used in the OMPS total column ozone algorithm. This value produces the observed amount of Rayleigh scattering (Ahmad et al., 2004) or atmospheric absorption (Koelemeijer et al., 2001) within the context of the MLER model.  $R_g$  is taken from a climatology developed from TOMS data with correction for areas of sunglint (C. Ahn, personal communication, 2009).

## OMPS Raman cloud algorithm

A. Vasilkov et al.

Title Page

Abstract

Introduction

Conclusions

References

Tables

Figures

◀

▶

◀

▶

Back

Close

Full Screen / Esc

Printer-friendly Version

Interactive Discussion



The first step in the cloud retrieval is to determine  $f$  by inverting Eq. (1) at a wavelength not substantially affected by rotational Raman scattering or atmospheric absorption (354.1 nm). We then retrieve the cloud OCP using the measured amount of filling-in and depletion of solar Fraunhofer line structure caused by RRS. The filling-in effect results in a high-frequency structure in the TOA radiance spectrum (Joiner et al., 1995). The cloud OCP is derived by a minimum-variance spectral fitting technique that minimizes the differences between the observed and computed high-frequency structure of TOA reflectance in the 345.5–354.5 nm range.

### 3.2 Rotational Raman scattering

The RRS spectral effects decrease with instrument spectral resolution. The OMPS NM sensor has a lower spectral resolution than the OMI. Therefore, the OMPS SO<sub>2</sub> and O<sub>3</sub> algorithms are less sensitive to effects of rotational Raman scattering (RRS) than their OMI counterparts. The cloud OMPS RRS algorithm will also be less sensitive to cloud pressure than OMI for a given signal to noise ratio.

Figure 1 compares the computed filling-in at the OMI and OMPS spectral resolutions. We compute inelastic RRS using the Linearized Discrete Ordinate Radiative Transfer (LIDORT-RRS) code (Spurr et al., 2008). LIDORT-RRS allows for accurate radiative transfer (RT) calculations in the presence of cloud/aerosol scattering. The RT computations were done for a solar zenith angle (SZA) of 45°, observation at nadir, and surface albedo of 0.05. Figure 1 clearly shows that the OMI filling-in is significantly higher than that computed at the OMPS resolution. However, even at the OMPS spectral resolution, the RRS filling-in is not negligible.

To compute the spectral effects of RRS, we use the fast table lookup approach that is implemented in the OMI algorithm and based on the approach of Joiner et al. (1995). In this approach, the fractional amounts of the various components of the radiance (according to a Lambertian surface model) are computed and stored for each iteration of scattering for a range of satellite and solar zenith angles, azimuth angles, and wavelengths (see Eq. 31 in Joiner et al., 1995). These radiance components are then

**OMPS Raman cloud algorithm**

A. Vasilkov et al.

Title Page

Abstract

Introduction

Conclusions

References

Tables

Figures

◀

▶

◀

▶

Back

Close

Full Screen / Esc

Printer-friendly Version

Interactive Discussion



linearly interpolated between nodes of the table. The radiative transfer calculations are carried out with the TOMRAD code based on successive iteration of the auxiliary equation in the theory of radiative transfer (Dave, 1964). The dependence upon surface reflectivity can be accounted for on the fly as described in Joiner et al. (1995) (see Eq. 31) and eliminates the need for an additional dimension in the table. This significantly reduces the amount of interpolation (and thus computational expense) needed for the table lookup approach.

Because the table parameters vary slowly and smoothly with wavelength, it is not necessary to provide them at high spectral resolution or sampling. The dependence of RRS filling-in on spectral resolution is accounted for by generating a secondary table for each individual instrument of the single scattered filling-in based on its measured solar irradiance spectrum as outlined in Joiner et al. (1995). In this approach, explicit knowledge of the instrument slit response function is not needed.

### 3.3 Detailed approach

Figure 2 (top) shows the post-launch (so-called Day 1) solar flux measurement from the OMPS NM sensor for the wavelength region used in our RRS cloud OCP retrieval. This measurement represents the average values of a series of solar flux measurements for the 36 cross-track fields-of-view (FOVs) taken every week during the first year of observation; since no discernible degradation in the diffuser was seen during this time period, the average provides a representative set of values to form the normalized radiances. In deriving the average, the Sun–Earth distance was accounted for, and the resulting measurement was normalized to 1 Astronomical Unit (AU). Additionally, because the solar flux is taken off a diffuser that is stepped over 7 different positions in order to illuminate the full CCD, measurements from the 7 different positions had to be stitched together using data from overlapping illuminated regions for each position.

A circular (loop) pattern is clearly evident in the measurements shown in Fig. 2. This pattern is partially due to the spectral smile caused by the sensor optics. The wavelength in the spectral dimension of the CCD varies along the CCD's spatial dimension;

## OMPS Raman cloud algorithm

A. Vasilkov et al.

Title Page

Abstract

Introduction

Conclusions

References

Tables

Figures

◀

▶

◀

▶

Back

Close

Full Screen / Esc

Printer-friendly Version

Interactive Discussion



for a given spatial row, it changes by approximately 0.2 nm from the edge of the CCD to the center, with the change being nearly symmetric about the center. The spectral resolution also varies as a function of cross-track position. The loops therefore denote the changes in wavelength and spectral resolution as the measurement goes from one edge of the CCD, to the center, and across to the other edge.

It should be emphasized that because both the OMPS radiance and irradiance measurements contain sensor effects (such as the spectral smile), they are meant to be used together to form the normalized radiance (ratio of radiance to irradiance). For the normalized radiances, the sensor effects largely cancel, and the resulting error, as compared with either radiance or irradiance measurements, is greatly reduced; analyses performed with the OMPS NM sensor indicate that the normalized radiance errors are generally less than 2%, well within instrument specification (Seftor et al., 2014).

For comparison, we produced a synthetic OMPS solar irradiance spectrum by convolving a high resolution solar spectrum (Chance and Kurucz, 2010) with measured OMPS band passes. Each cross track position has a different set of wavelengths and a different slit function. The expected OMPS solar flux is shown in Fig. 2 (bottom) using dots for each cross-track position. It is seen that the OMPS band passes noticeably vary with cross-track position resulting in wavelength shifts. If band passes were constant, the curve would be smooth and there would be no circular behavior. This plot shows the expected looping due to band pass variation across the swath and a changing wavelength grid.

There are significant differences between the observed and simulated OMPS solar irradiance spectra. The measured solar data have a larger loop pattern as compared with the synthetic data and also show more spectral discontinuity, potentially causing problems for spectral interpolation (for a given cross-track position). These differences between the observed and simulated OMPS solar spectra are mostly due to calibration errors. Radiometric requirements that allow OMPS to meet the specified ozone accuracy and precision are based on a normalized radiance, which is the ratio of measured Earth radiance to measured solar irradiance. The solar irradiance is measured



the OMPS normalized radiances to the predefined table wavelengths. Note again that the OMPS wavelengths vary as a function of cross-track position. Similar patterns are seen in OMI-derived radiance residuals (Joiner and Vasilkov, 2006).

## 4 Results

### 4.1 Comparison of OMI and OMPS cloud products

Figure 4 (top) shows a map of cloud OCPs retrieved from OMPS measurements on 7 January 2013. Data with effective cloud fraction greater than 0.05 are shown, as cloud pressure retrievals are not performed for cloud fractions  $< 0.05$ . Similarly, Fig. 4 (bottom) shows a map of cloud OCP retrieved from OMI measurements on the same day. OMI data affected by interference from material outside the instrument, known as the “row anomaly”, were removed. A visual comparison of two maps suggests that there is good qualitative agreement between the spatial distribution of OCP derived from OMI and OMPS. For instance, areas with high altitude clouds over the northern Pacific ocean, Mexico, the northern Atlantic ocean, northern China, etc., look quite similar. However, there are some quantitative differences, for instance, in the oceanic tropics where OMI displays more low pressure OCPs than OMPS. Figure 4 (top) shows that the rightmost OMPS swath position has a significant error (unrealistically low cloud pressures). The precise cause of this error has not yet been identified. We remove data from this swath position in all subsequent analysis.

To compare the cloud products retrieved from OMPS and OMI quantitatively, we use probability density functions (PDFs) of effective cloud fraction (ECF) and OCP calculated for different latitude and ECF bins. A direct one-to-one comparison cannot be accomplished owing to the different spatial resolutions of OMI and OMPS and the fact that observations are not made at precisely the same times. Figure 5 shows a comparison of PDFs of OMPS and OMI effective cloud fractions for the tropics. The PDFs of OMPS and OMI effective cloud fractions are practically identical. Even if we assume

## OMPS Raman cloud algorithm

A. Vasilkov et al.

Title Page

Abstract

Introduction

Conclusions

References

Tables

Figures

◀

▶

◀

▶

Back

Close

Full Screen / Esc

Printer-friendly Version

Interactive Discussion



**OMPS Raman cloud algorithm**

A. Vasilkov et al.

Title Page

Abstract

Introduction

Conclusions

References

Tables

Figures

◀

▶

◀

▶

Back

Close

Full Screen / Esc

Printer-friendly Version

Interactive Discussion



that radiometric calibration of both OMI and OMPS is perfect, we might expect some differences in the derived ECFs owing to of the different sizes of the OMI and OMPS footprints. It is reasonable to anticipate more cases of higher cloud fraction for the smaller OMI footprints. However, the PDFs of the OMI and OMPS ECF appear to be very close each other. This comparison allows us to state that there is good confidence in the OMPS ECF product and in the OMPS calibration since much work and validation has already been done for the OMI calibration (Dobber et al., 2006, 2008).

Figure 6 shows a comparison of PDFs of OCP retrieved from OMI and OMPS over the tropics and northern and southern mid-latitudes for scenes with  $ECF > 0.3$ . OMI pixels affected by the row anomaly were excluded from the comparison. The comparison of the PDFs is similar to that carried out in Joiner et al. (2012); it is intended to evaluate the OMPS OCP retrievals for moderately to highly cloudy conditions. In general, the PDFs from OMI and OMPS cloud pressures qualitatively agree. However, OMPS retrieves higher cloud pressures more often than OMI does. Particularly, this is true for the tropics. A simple visual comparison of the maps in Fig. 4 reveals lower OMI cloud pressures in the tropics. Note that the peak near 1000 hPa in the Southern Hemisphere is likely due to scenes with ice or snow in them.

A possible cause of higher cloud pressure retrieved by OMPS could be related to the effects of stray light contributions to TOA radiances in OMPS. The TOA radiance measured by the OMPS NM sensor is not corrected for stray light contributions, whereas a stray light correction is applied for OMI. Stray light is an additive error to the measured TOA radiance and leads to erroneous filling-in of Earth-shine Fraunhofer lines. This additional filling-in due to stray light results in higher cloud pressure retrievals because the retrieved cloud pressure is approximately proportional to the filling-in of Earth-shine Fraunhofer lines.

We ran an additional experiment using a version of the OMPS level 1b data with a proposed stray light correction. We found that the PDFs were not substantially different from those in Fig. 6. This means that either stray light in OMPS is not the root cause of the differences between OMPS and OMI or that the stray light corrections in

OMPS (and/or OMI) are not sufficient for the cloud algorithm. We intend to examine this issue further in the future.

OMI RRS OCP retrievals have also been compared with coincident OMI retrievals using oxygen dimer absorption (Sneep et al., 2008; Joiner et al., 2012) and predicted values based on a fast simulation using cloud optical thickness profiles derived from CloudSat radar reflectivity profiles and radiances from the MODerate-resolution Imaging Spectroradiometer (Vasilkov et al., 2008; Joiner et al., 2012). Although these comparisons were relatively good, some differences (within the range of the OMI and OMPS differences seen here) were noted; it was not clear how to attribute those differences to errors in the various instruments and algorithms as there is no clearly defined gold-standard for validation. Therefore, we similarly are not able attribute the OMI-OMPS differences seen here to errors one instrument or the other.

To evaluate the OMPS-derived OCP product, it is useful to analyze differences between surface pressure and OCP,  $\Delta P = P_s - P_c$ , for mostly clear-sky conditions where a scene pressure is retrieved. For those conditions, the retrieved OCP should be close to the surface pressure, i.e. this difference should be small. We calculated a mean  $\Delta P$  of  $-1.7$  hPa and standard deviation  $\sigma = 46.2$  hPa using OMPS cloud retrievals from the Antarctic plateau region on 7 January 2013. The small mean value indicates that the soft calibration of TOA radiances (based on OMPS data of 21 December 2012) works well. In comparison, for OMI we find a mean  $\Delta P$  of  $-15.3$  hPa and  $\sigma = 36.0$  hPa indicating a slightly lower random errors in OMI as compared with OMPS.

## 4.2 Effects of the OMPS-retrieved cloud OCP on total column ozone

The current NASA OMPS research total ozone algorithm is based on the heritage algorithm designed for the Total Ozone Mapping Spectrometer (TOMS) series of satellite instrument and also applied to OMI (McPeters et al., 2013). Initial studies show that the algorithm is performing with expected quality for OMPS (Kramarova et al., 2013; Bai et al., 2013), similar to that of the well-validated OMI-TOMS algorithm (McPeters et al., 2008). The NASA OMPS total ozone algorithm currently makes use of a monthly

## OMPS Raman cloud algorithm

A. Vasilkov et al.

Title Page

Abstract

Introduction

Conclusions

References

Tables

Figures

◀

▶

◀

▶

Back

Close

Full Screen / Esc

Printer-friendly Version

Interactive Discussion



gridded cloud OCP climatology derived from OMI-retrieved cloud OCPs. This climatology was also developed for use in the reprocessing of historical TOMS data.

Here, we compare OMPS total column ozone retrievals derived with the cloud OCP climatology and actual cloud OCPs. Figure 7 shows percentage differences between the standard NASA OMPS total ozone product and total ozone retrieved with using OMPS-derived cloud OCPs. For comparison, the OMPS-derived reflectivity is also shown, indicating areas of heavy cloud cover. We note that ozone differences are very small for the overwhelming majority of the globe. Ozone differences are mostly positive and can be up to  $\sim 5\%$ . They are well correlated with bright clouds over the ocean as can be seen from a visual comparison in Fig. 7. Negative ozone differences over the northern Atlantic ocean are also correlated with bright clouds. All of the total ozone differences in Fig. 7 are caused by the fact that the actual cloud OCPs deviate from the monthly gridded climatology.

Figure 8 compares OMPS and OMI total ozone retrievals, where OMPS retrievals are performed with either the OMI cloud OCP climatology (top) or using actual OMPS-derived cloud OCPs (bottom). For total column ozone, having an exact matchup in both time and space is not as critical as it is for cloud retrievals. The comparison is performed for 7 January 2013 in locations not affected by the OMI row anomaly. Because the OMPS retrievals use a different set of ozone cross sections than those used for the OMI retrievals, we processed OMPS data with the OMI ozone cross sections (Bass and Paur, 1985). The left panels of Fig. 8 show the spatial distribution of the percentage differences between OMPS and OMI total ozone retrievals and the right panels show histograms of those differences along with an approximation of the histograms using a Gaussian function.

The mean ozone difference in both cases is well within 1 %, becoming slightly worse with the use of colocated OCP retrievals. This is most likely due to the fact that, as discussed above, the OMPS-derived OCP is higher on average than the OMI-derived OCP; this, in turn, slightly reduces the ozone retrieved by OMPS in comparison with that from OMI. However, it should also be noted that the width of the

## OMPS Raman cloud algorithm

A. Vasilkov et al.

Title Page

Abstract

Introduction

Conclusions

References

Tables

Figures

◀

▶

◀

▶

Back

Close

Full Screen / Esc

Printer-friendly Version

Interactive Discussion



difference distribution decreases slightly when the colocated OCPs are used, from 1.09 % to 1.05 %, indicating a slightly better correlation. Furthermore, areas with heavy cloud cover (e.g., over the Pacific Ocean and South America) visually show smaller OMPS/OMI differences in Fig. 8 when the colocated OCP retrievals are used.

## 5 Conclusions

We have reworked the OMI cloud OCP algorithm to handle OMPS data. Key elements of the OMPS cloud pressure algorithm include the use of soft calibration of TOA radiances, the use of a synthetic high resolution solar flux for generation of the RRS lookup tables, and spline interpolation of the TOA radiances over the lookup table wavelength grid. We find that the PDFs of effective cloud fraction retrieved from OMPS and well-validated OMI measurements are very close to each other, indicating excellent calibration of OMPS normalized radiances. The PDFs of the OMPS and OMI OCPs are similar; however, OMPS retrieves a somewhat higher OCP on average. These differences are still under investigation.

The use of actual OMPS cloud OCPs, as compared with the use of an OMI-derived monthly gridded cloud OCP climatology, brings total column  $O_3$  estimates into slightly better agreement with OMI. However, the monthly gridded OMI cloud OCP climatology captures much of the variability in OCP. Total column  $O_3$  from OMPS appears to be quite good (by comparison with well-validated OMI retrrievals) when the OMI-based cloud OCP climatology is used.

*Acknowledgements.* Funding for this work was provided in part by the NASA NPP Science Team for Climate Data Records program (NNH10ZDA001N) managed by Diane Wickland; we significantly leveraged our algorithm development experience funded by the NASA Aura science team. We thank P. K. Bhartia, R. D. McPeters, N. Krotkov, and K. Yang for helpful discussions. We particularly thank Jason Li for processing OMPS data used for comparisons of OMPS and OMI total ozone.

## OMPS Raman cloud algorithm

A. Vasilkov et al.

Title Page

Abstract

Introduction

Conclusions

References

Tables

Figures

◀

▶

◀

▶

Back

Close

Full Screen / Esc

Printer-friendly Version

Interactive Discussion



## References

- Ahmad, Z., Bhartia, P. K., and Krotkov, N.: Spectral properties of backscattered UV radiation in cloudy atmospheres, *J. Geophys. Res.*, 109, D01201, doi:10.1029/2003JD003395, 2004. 2693
- 5 Bai, K., Liu, C., Shi, R., and Gao, W.: Validation of the Suomi NPP Ozone Mapping and Profiler Suite total column ozone using Brewer and Dobson spectrophotometers, *Atmos. Meas. Tech. Discuss.*, 6, 4577–4605, doi:10.5194/amtd-6-4577-2013, 2013. 2700
- Bass, A. M. and Paur, R. J.: The ultraviolet cross-sections of ozone, in: *Atmospheric Ozone*, edited by: Zerefos, C. Z., and Ghaz, A., D. Reidel, Norwell, Mass., 606–616, 1985. 2701
- 10 Chance, K. and Kurucz, R. L.: An improved high-resolution solar reference spectrum for Earth's atmosphere measurements in the ultraviolet, visible, and near infrared, *J. Quant. Spectrosc. Ra.*, 111, 1289–1295, 2010. 2696
- Dave, J. V.: Meaning of successive iteration of the auxiliary equation of radiative transfer, *Astrophys. J.*, 140, 1292–1303, 1964. 2695
- 15 Dobber, M. R., Dirksen, R., Levelt, P., van den Oord, G. H. J., Voors, R., Kleipool, Q., Jaross, G., Kowalewski, M., Hilsenrath, E., Leppelmeier, G., de Vries, J., Dierssen, W., and Rozemeijer, N.: Ozone monitoring instrument calibration, *IEEE T. Geosci. Remote*, 44, 1209–1238, doi:10.1109/TGRS.2006.869987, 2006. 2699
- Dobber, M. R., Kleipool, Q., Dirksen, R., Levelt, P., Jaross, G., Taylor, S., Kelly, T., Flynn, L. E., Leppelmeier, G., and Rozemeijer, N.: Validation of ozone monitoring instrument level-1b data products, *J. Geophys. Res.*, 113, D15S06, doi:10.1029/2007JD008665, 2008. 2699
- 20 Ferlay, N., Thieuleux, F., Cornet, C., Davis, A. B., Dubuisson, P., Ducos, F., Parol, F., Riédi, J., and Vanbauce, C.: Toward new inferences about cloud structures from multidirectional measurements in the Oxygen A Band: middle-of-cloud pressure and cloud geometrical thickness from POLDER-3/PARASOL, *J. Appl. Meteorol. Clim.*, 49, 2492–2507, doi:10.1175/2010JAMC2550.1, 2010. 2691
- 25 Flynn, L. E., Seftor, C. J., Larsen, J. C., and Xu, P.: The ozone mapping and profiler suite, in: *Earth Science Satellite Remote Sensing*, edited by: Qu, J. J., Gao, W., Kafatos, M., Murphy, R. E., and Salomonson, V. V., Springer, Berlin, 279–296, doi:10.1007/978-3-540-37293-6, 2006. 2692
- 30 Flynn, L., Long, C., Wu, X., Evans, R., Beck, C. T., Petropavlovskikh, I., McConville, G., Yu, W., Zhang, A., Niu, J., Beach, E., Hao, Y., Pan, C., Sen, B., Novicki, M., Zhou, S., and Seftor, C.:

## OMPS Raman cloud algorithm

A. Vasilkov et al.

Title Page

Abstract

Introduction

Conclusions

References

Tables

Figures

◀

▶

◀

▶

Back

Close

Full Screen / Esc

Printer-friendly Version

Interactive Discussion



## OMPS Raman cloud algorithm

A. Vasilkov et al.

Title Page

Abstract

Introduction

Conclusions

References

Tables

Figures

◀

▶

◀

▶

Back

Close

Full Screen / Esc

Printer-friendly Version

Interactive Discussion



Performance of the ozone mapping and profiler suite (OMPS) products, *J. Geophys. Res.*, online first, doi:10.1002/2013JD020472, 2014.

Joiner, J. and Vasilkov, A. P.: First results from the OMI Rotational-Raman scattering cloud pressure algorithm, *IEEE T. Geosci. Remote*, 44, 1272–1282, 2006. 2693, 2698

5 Joiner, J., Bhartia, P. K., Cebula, R. P., Hilsenrath, E., McPeters, R. D., and Park, H.: Rotational-Raman scattering (Ring effect) in satellite backscatter ultraviolet measurements, *Appl. Optics*, 34, 4513–4525, 1995. 2694, 2695

Joiner, J., Vasilkov, A. P., Flittner, D. E., Gleason, J. F., and Bhartia, P. K.: Retrieval of cloud chlorophyll content using Raman scattering in GOME spectra, *J. Geophys. Res.*, 109, D01109, doi:10.1029/2003JD003698, 2004. 2693

10 Joiner, J., Vasilkov, A. P., Yang, K., and Bhartia, P. K.: Total column ozone over hurricanes from the ozone monitoring instrument, *Geophys. Res. Lett.*, 33, L06807, doi:10.1029/2005GL025592, 2006. 2691

15 Joiner, J., Schoeberl, M. R., Vasilkov, A. P., Oreopoulos, L., Platnick, S., Livesey, N. J., and Levelt, P. F.: Accurate satellite-derived estimates of the tropospheric ozone impact on the global radiation budget, *Atmos. Chem. Phys.*, 9, 4447–4465, doi:10.5194/acp-9-4447-2009, 2009. 2691

20 Joiner, J., Vasilkov, A. P., Bhartia, P. K., Wind, G., Platnick, S., and Menzel, W. P.: Detection of multi-layer and vertically-extended clouds using A-train sensors, *Atmos. Meas. Tech.*, 3, 233–247, doi:10.5194/amt-3-233-2010, 2010. 2691

Joiner, J., Vasilkov, A. P., Gupta, P., Bhartia, P. K., Veeffkind, P., Sneep, M., de Haan, J., Polonsky, I., and Spurr, R.: Fast simulators for satellite cloud optical centroid pressure retrievals; evaluation of OMI cloud retrievals, *Atmos. Meas. Tech.*, 5, 529–545, doi:10.5194/amt-5-529-2012, 2012. 2691, 2699, 2700

25 Koelmeijer, R. B. A., Stammes, P., Hovenier, J. W., and de Haan, J. F.: A fast method for retrieval of cloud parameters using oxygen A-band measurements from the Global Ozone Monitoring Experiment, *J. Geophys. Res.*, 106, 3475–3496, 2001. 2693

30 Kramarova, N. A., Nash, E. R., Newman, P. A., Bhartia, P. K., McPeters, R. D., Rault, D. F., Seftor, C. J., and Xu, P. Q.: Measuring the Antarctic ozone hole with the new Ozone Mapping and Profiler Suite (OMPS), *Atmos. Chem. Phys. Discuss.*, 13, 26305–26325, doi:10.5194/acpd-13-26305-2013, 2013. 2700

## OMPS Raman cloud algorithm

A. Vasilkov et al.

Title Page

Abstract

Introduction

Conclusions

References

Tables

Figures

◀

▶

◀

▶

Back

Close

Full Screen / Esc

Printer-friendly Version

Interactive Discussion



- Levelt, P. F., van der Oord, G. H. J., Dobber, M. R., Malkki, A., Visser, H., de Vries, J., Stammes, P., Lundell, J. O. V., and Saari, H.: The ozone monitoring instrument, *IEEE T. Geosci. Remote*, 44, 1093–1101, 2006. 2692
- 5 McPeters, R., Kroon, M., Labow, G., Brinksma, E., Balis, D., Petropavlovskikh, I., Veefkind, J. P., Bhartia, P. K., and Levelt, P. F.: Validation of the Aura ozone monitoring instrument total column ozone product, *J. Geophys. Res.*, 113, D15S14, doi:10.1029/2007JD008802, 2008. 2700
- 10 McPeters, R. D., Seftor, C., Jaross, G., Li, J., Yang, K., Krotkov, N., Joiner, J., Vasilkov, A. P., and Haffner, D.: A status report to NASA headquarters of the OMPS science team evaluation, available at: [http://npp.gsfc.nasa.gov/DEW\\_NPP\\_reports/OMPS%20Nadir%20Products%20Report%20\(Jan-22-2013\).pdf](http://npp.gsfc.nasa.gov/DEW_NPP_reports/OMPS%20Nadir%20Products%20Report%20(Jan-22-2013).pdf) (last access: 13 March 2014), 2013. 2691, 2700
- 15 Rozanov, V. V., Kokhanovsky, A. A., and Burrows, J. P.: The determination of cloud altitudes using GOME reflectance spectra: multilayered cloud systems, *IEEE T. Geosci. Remote*, 42, 1009–1017, 2004. 2691
- 20 Seftor, C. J., Jaross, G., Kowitt, M., Haken, M., Li, J., and Flynn, L. E.: Post-launch performance of the Suomi NPP ozone mapping and profiler, *J. Geophys. Res.*, online first, doi:10.1002/2013JD020472, 2014. 2696, 2697
- 25 Sneep, M., de Haan, J., Stammes, P., Wang, P., Vanbauce, C., Joiner, J., Vasilkov, A. P., and Levelt, P. F.: Three way comparison between OMI/Aura and POLDER/PARASOL cloud pressure products, *J. Geophys. Res.*, 113, D15S23, doi:10.1029/2007JD008694, 2008. 2700
- Spurr, R. J. D., de Haan, J., van Oss, R., and Vasilkov, A. P.: Discrete ordinate radiative transfer in a stratified medium with first order rotational Raman scattering, *J. Quant. Spectrosc. Ra.*, 109, 404–425, 2008. 2694
- 30 Stammes, P., Sneep, M., de Haan, J. F., Veefkind, J. P., Wang, P., and Levelt, P. F.: Effective cloud fractions from the Ozone Monitoring Instrument: theoretical framework and validation, *J. Geophys. Res.*, 113, D16S38, doi:10.1029/2007JD008820, 2008. 2693
- Vasilkov, A. P., Joiner, J., Yang, K., and Bhartia, P. K.: Improving total column ozone retrievals by using cloud pressures derived from Raman scattering in the UV, *Geophys. Res. Lett.*, 31, L20109, doi:10.1029/2004GL020603, 2004. 2691
- Vasilkov, A. P., Joiner, J., Spurr, R., Bhartia, P. K., Levelt, P. F., and Stephens, G.: Evaluation of the OMI cloud pressures derived from rotational Raman scattering by comparisons



**OMPS Raman cloud  
algorithm**

A. Vasilkov et al.

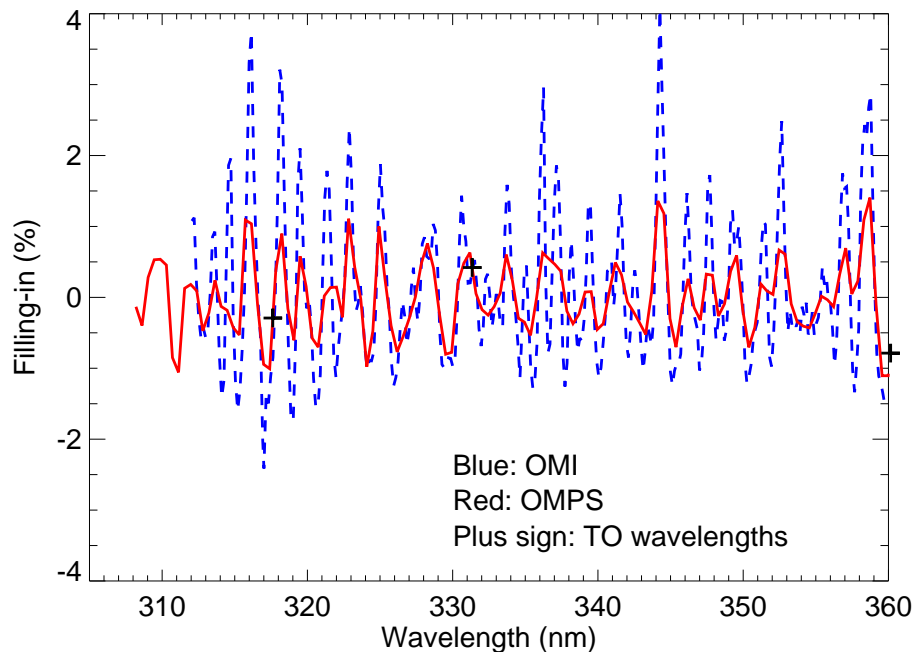


**Fig. 1.** Comparison of OMI and OMPS RRS filling-ins. Plus signs show the wavelengths used in the OMPS total ozone (TO) algorithm.

[Title Page](#)[Abstract](#)[Introduction](#)[Conclusions](#)[References](#)[Tables](#)[Figures](#)[◀](#)[▶](#)[◀](#)[▶](#)[Back](#)[Close](#)[Full Screen / Esc](#)[Printer-friendly Version](#)[Interactive Discussion](#)

**OMPS Raman cloud  
algorithm**

A. Vasilkov et al.

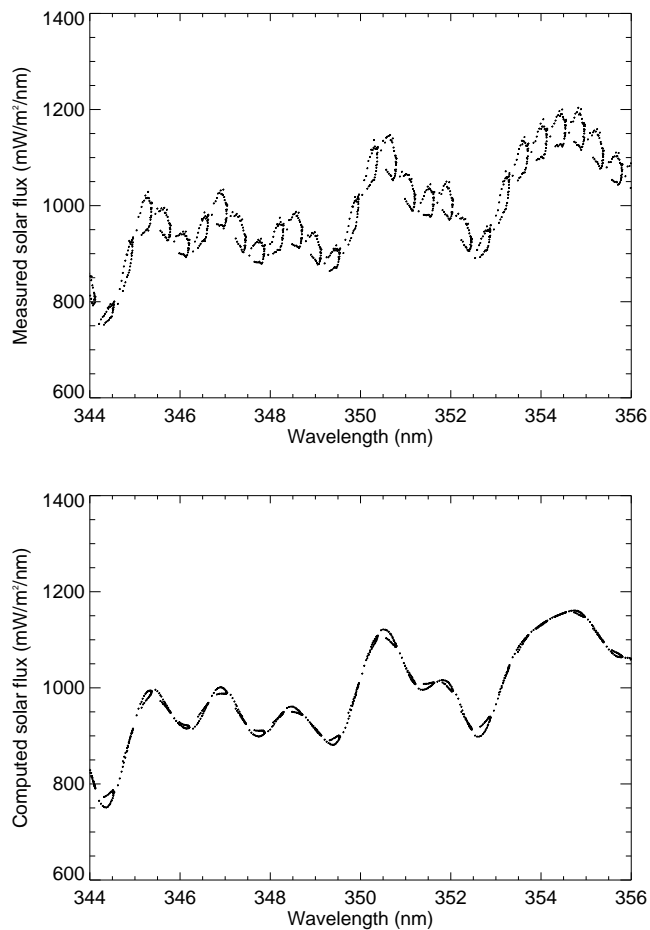


**Fig. 2.** OMPS-measured solar flux (top) and high resolution solar flux convolved with the measured OMPS NM band-passes (bottom). Dots are for different cross-track positions.

**OMPS Raman cloud algorithm**

A. Vasilkov et al.

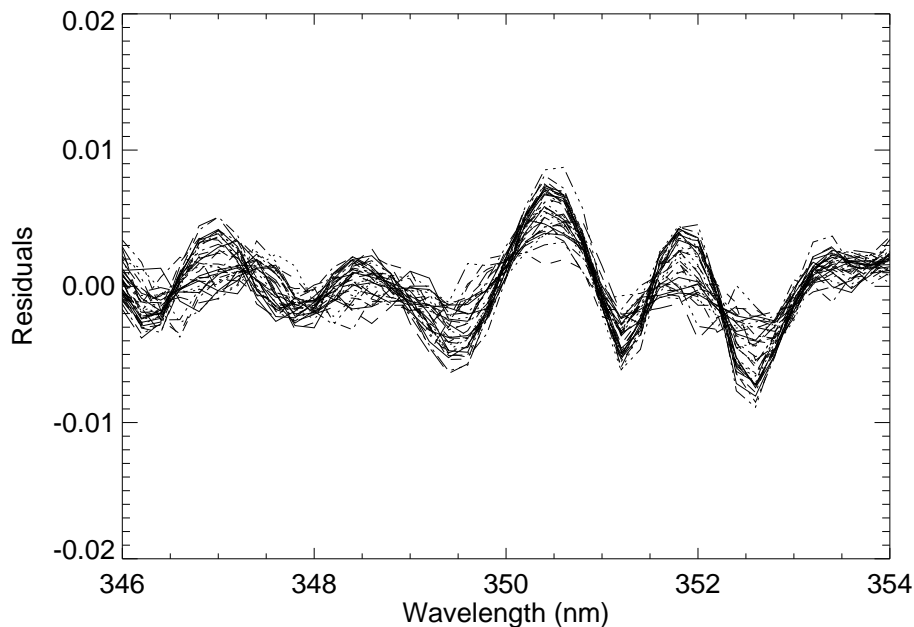


**Fig. 3.** Spectral residuals/corrections that are applied to measured TOA OMPS radiances as derived from data over Antarctica. Each curve is for a particular OMPS scan position.

[Title Page](#)[Abstract](#)[Introduction](#)[Conclusions](#)[References](#)[Tables](#)[Figures](#)[◀](#)[▶](#)[◀](#)[▶](#)[Back](#)[Close](#)[Full Screen / Esc](#)[Printer-friendly Version](#)[Interactive Discussion](#)

OMPS Raman cloud  
algorithm

A. Vasilkov et al.

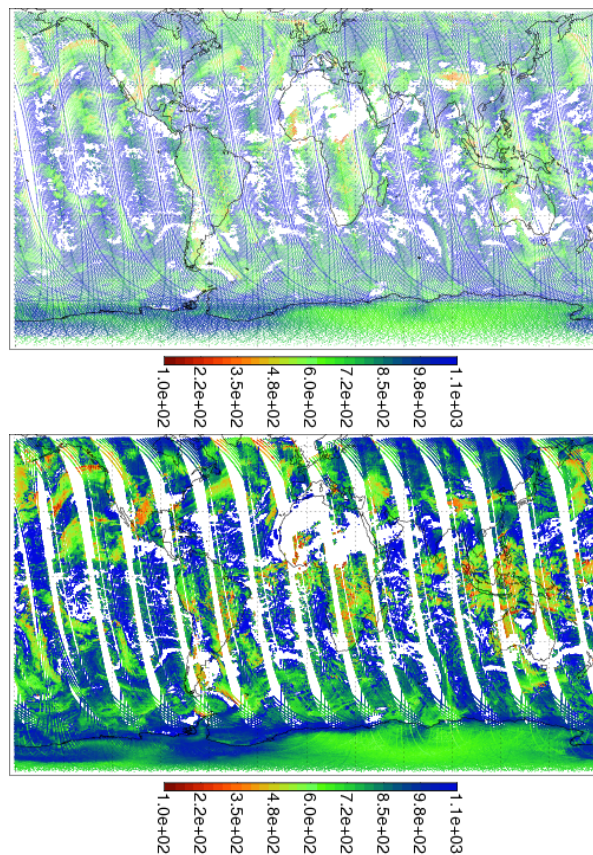


**Fig. 4.** OCP (in hPa) from OMPS measurements (top) and OMI measurements (bottom) on 7 January 2013. Every pixel on the maps is represented by a color dot. OMI has 60 cross track pixels while OMPS has 36 pixels. More pixels leads to a visual effect of the OMI map being brighter than the OMPS map.

Title Page

Abstract

Introduction

Conclusions

References

Tables

Figures

◀

▶

◀

▶

Back

Close

Full Screen / Esc

Printer-friendly Version

Interactive Discussion



## OMPS Raman cloud algorithm

A. Vasilkov et al.

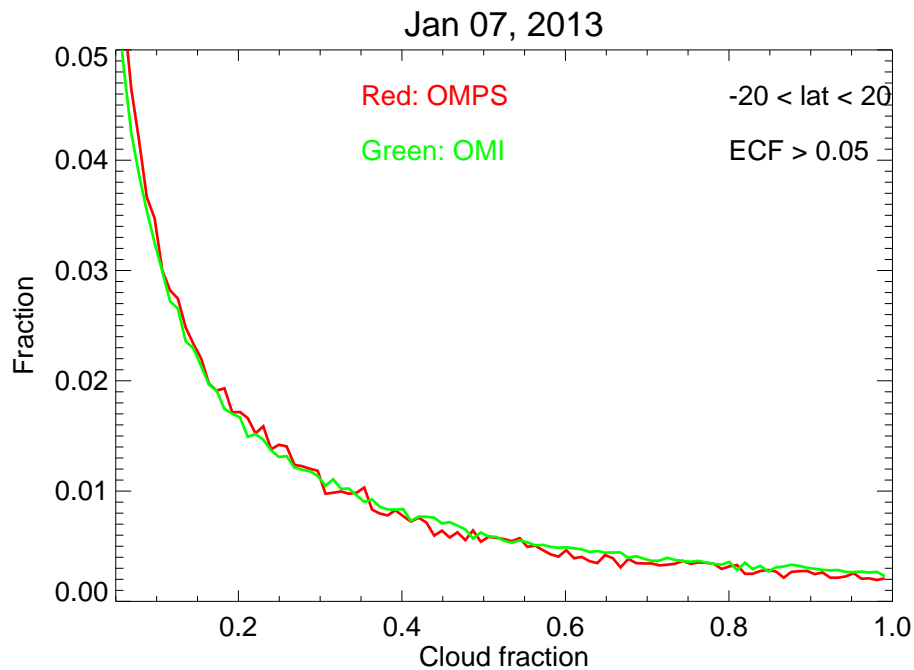
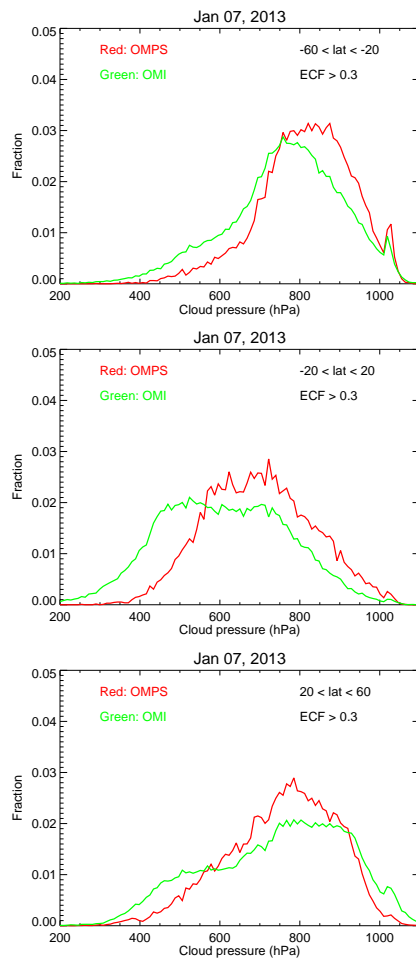


Fig. 5. Probability density functions of OMPS and OMI effective cloud fractions for the tropics.

[Title Page](#)[Abstract](#)[Introduction](#)[Conclusions](#)[References](#)[Tables](#)[Figures](#)[◀](#)[▶](#)[◀](#)[▶](#)[Back](#)[Close](#)[Full Screen / Esc](#)[Printer-friendly Version](#)[Interactive Discussion](#)

## OMPS Raman cloud algorithm

A. Vasilkov et al.



**Fig. 6.** Probability density functions of OMPS and OMI cloud pressures for three latitude bins: southern mid-latitudes (top), tropics (middle), and northern mid-latitudes (bottom).

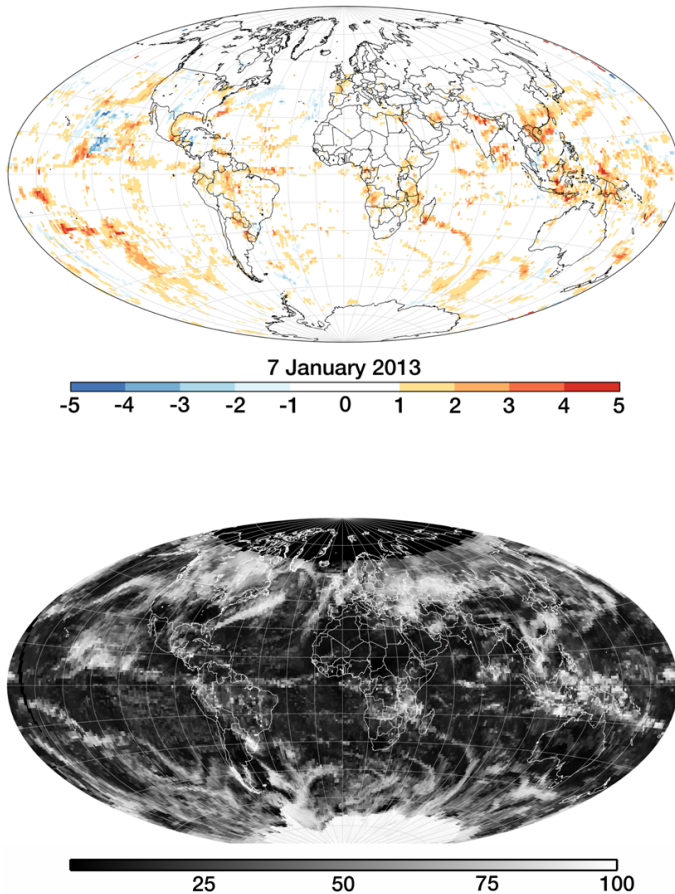


**Fig. 7.** Total ozone differences (in %) due to the use of retrieved cloud OCPs instead of the OMI cloud OCP climatology (top) and OMPS-derived reflectivity (in %) at 331 nm for 7 January 2013 (bottom).

**OMPS Raman cloud algorithm**

A. Vasilkov et al.

Title Page

Abstract Introduction

Conclusions References

Tables Figures

◀ ▶

◀ ▶

Back Close

Full Screen / Esc

Printer-friendly Version

Interactive Discussion



## OMPS Raman cloud algorithm

A. Vasilkov et al.

Title Page

Abstract

Introduction

Conclusions

References

Tables

Figures

◀

▶

◀

▶

Back

Close

Full Screen / Esc

Printer-friendly Version

Interactive Discussion

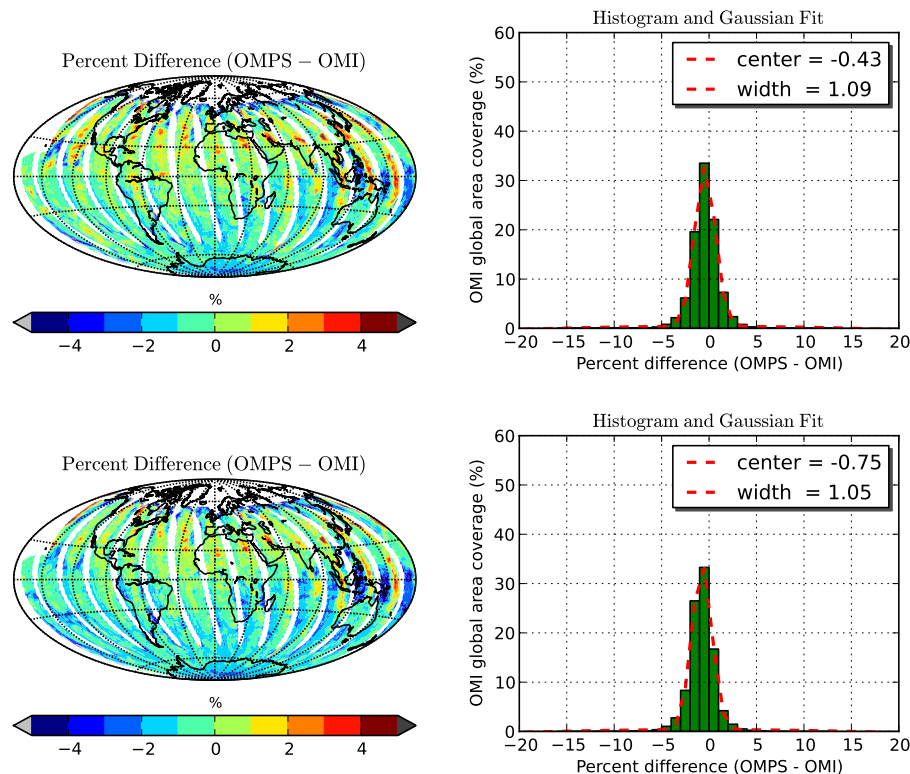


**Fig. 8.** Total ozone differences between OMPS and OMI on 7 January 2013 with the use of the cloud OCP climatology (top) and the retrieved cloud OCP (bottom). The left panels show spatial distributions of the total ozone differences; the right panels show histograms of total ozone differences and their approximation with a Gaussian function.